Aalto University

OPEN ACCESS

This is an electronic reprint of the original article.
This reprint may differ from the original in pagination and typographic detail.

Chen, Guangze; Chen, Wei; Zilberberg, Oded

Field-effect transistor based on surface negative refraction in Weyl nanowire

Published in:
APL Materials

DOI:
10.1063/1.5126033

Published: 01/01/2020

Document Version
Publisher's PDF, also known as Version of record

Published under the following license:
CC BY

Please cite the original version:
Chen, G., Chen, W., & Zilberberg, O. (2020). Field-effect transistor based on surface negative refraction in Weyl nanowire. *APL Materials*, *8*(1), 1-6. Article 011102. https://doi.org/10.1063/1.5126033

This material is protected by copyright and other intellectual property rights, and duplication or sale of all or part of any of the repository collections is not permitted, except that material may be duplicated by you for your research use or educational purposes in electronic or print form. You must obtain permission for any other use. Electronic or print copies may not be offered, whether for sale or otherwise to anyone who is not an authorised user.

APL Materials

Field-effect transistor based on surface negative refraction in Weyl nanowire

Cite as: APL Mater. **8**, 011102 (2020); https://doi.org/10.1063/1.5126033
Submitted: 28 August 2019 . Accepted: 15 December 2019 . Published Online: 06 January 2020

Guangze Chen, Wei Chen, and Oded Zilberberg

COLLECTIONS

Paper published as part of the special topic on Topological Semimetals — New Directions
Note: This paper is part of the Special Topic on Topological Semimetals–New Directions.

View Online Export Citation CrossMark

ARTICLES YOU MAY BE INTERESTED IN

Inverse-perovskites A_3BO (A = Sr, Ca, Eu/B = Pb, Sn): A platform for control of Dirac and Weyl Fermions
APL Materials **7**, 121114 (2019); https://doi.org/10.1063/1.5129695

Epitaxial strain and the magnetic properties of canted antiferromagnetic perovskite $NaNiF_3$ thin films
APL Materials **8**, 011101 (2020); https://doi.org/10.1063/1.5126601

Synthesis and resistivity of topological metal MoP nanostructures
APL Materials **8**, 011103 (2020); https://doi.org/10.1063/1.5130159

© 2020 Author(s).

Field-effect transistor based on surface negative refraction in Weyl nanowire

Cite as: APL Mater. 8, 011102 (2020); doi: 10.1063/1.5126033
Submitted: 28 August 2019 • Accepted: 15 December 2019 •
Published Online: 6 January 2020

View Online Export Citation CrossMark

Guangze Chen,[1,2] Wei Chen,[1,3,4,a)] and Oded Zilberberg[1]

AFFILIATIONS

[1]Institute for Theoretical Physics, ETH Zurich, 8093 Zurich, Switzerland
[2]Department of Applied Physics, Aalto University, 02150 Espoo, Finland
[3]National Laboratory of Solid State Microstructures and School of Physics, Nanjing University, Nanjing 210093, China
[4]College of Science, Nanjing University of Aeronautics and Astronautics, Nanjing 210016, China

Note: This paper is part of the Special Topic on Topological Semimetals—New Directions.
[a)]**Electronic mail:** pchenweis@gmail.com

ABSTRACT

Weyl semimetals are characterized by their bulk Weyl points—conical band touching points that carry a topological monopole charge—and Fermi arc states that span between the Weyl points on the surface of the material. Recently, significant progress has been made toward the understanding and measurement of the physical properties of Weyl semimetals. Yet, potential applications remain relatively sparse. Here we propose Weyl semimetal nanowires as field-effect transistors, dubbed WEYLFETs. Specifically, applying gradient gate voltage along the nanowire, an electric field is generated, which effectively tilts the open surfaces, thus, varying the relative orientation between Fermi arcs on different surfaces. As a result, perfect negative refraction between adjacent surfaces can occur and longitudinal conductance along the wire is suppressed. The WEYLFET offers a high on/off ratio with low power consumption. Adverse effects due to dispersive Fermi arcs and surface disorder are studied.

© 2020 Author(s). All article content, except where otherwise noted, is licensed under a Creative Commons Attribution (CC BY) license (http://creativecommons.org/licenses/by/4.0/). https://doi.org/10.1063/1.5126033

Field-effect transistors (FETs) are electronic devices that use an electric field to control the flow of current through the device.[1] There is a wide variety of materials and platforms used for various cases of FETs; the majority thereof relies on semiconductor devices where the conduction channel can be switched off using an external gate. The conduction channel lies in the bulk of the semiconductor and early challenges in FET production concerned with surface passivation in order to overcome surface effects that prevented the gating from reaching the bulk.[1] In parallel, low-power FETs' applications are in constant development where new materials and reduced dimensionality of the conduction channel play a crucial role.[2,3] Most recently, the progress of topological materials has opened a new avenue toward this goal based on the dissipationless chiral edge channels of the quantum anomalous Hall effect.[4–11]

Weyl semimetals are a class of 3D materials with conduction and valence bands that linearly touch at isolated points of the bulk spectrum.[12–17] The touching points are the so-called Weyl points around which the electronic states can be effectively described by the Weyl equation.[12] Each Weyl point carries a monopole charge of Berry curvature, thus splitting the momentum space into different regions of gapped spectra with different topologies.[12,18] These unique bulk properties lead to electron chirality, which offers potential applications such as a bulk photovoltaic effect.[19,20]

In parallel, the nontrivial bulk topology has a corresponding boundary effect in the form of Fermi arcs that appear in the surface Brillouin zone,[12] which were recently observed experimentally.[21–32] These arcs have an open cut at the chemical potential, leading to directional transport on the surface. Furthermore, depending on the orientation of the surface, the Fermi arcs are projected from the bulk Weyl points differently.[33] This can lead to tunable surface configurations where negative refraction may occur between different surfaces of the material.[34]

In this letter, we propose a new type of FET based on field-controlled surface negative refraction in a Weyl nanowire or, in short, a WEYLFET. We consider a Weyl semimetal nanowire covered by isolated metal gates on top of each surface [see Fig. 1(a)].

© Author(s) 2020

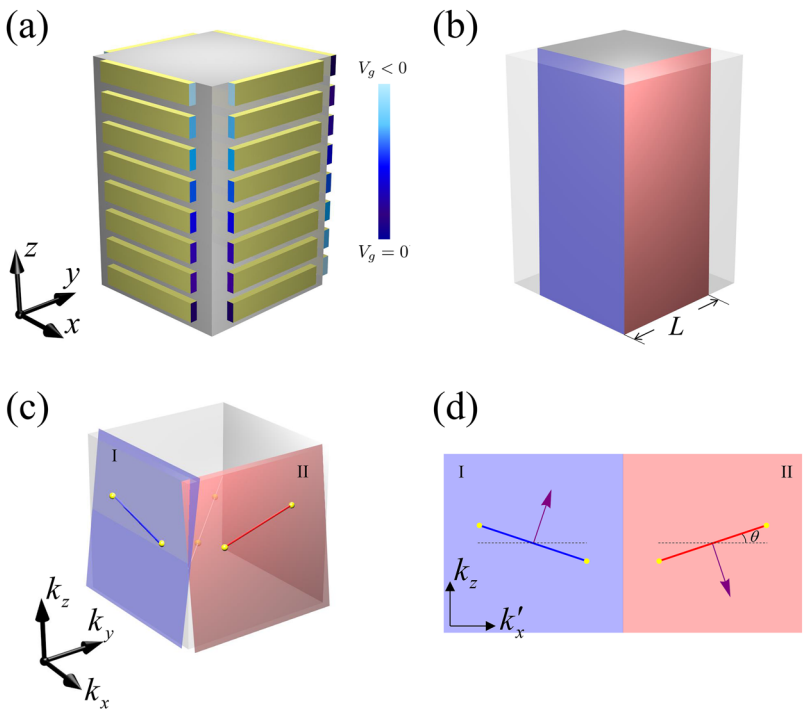

FIG. 1. Schematic of the Weyl semimetal field-effect transistor (WEYLFET). (a) The device is made of a Weyl semimetal nanowire (bulk core). Isolated metal gates are fabricated on top of the wire's surfaces with opposite gate-voltage gradients on the front and back surfaces (mind the color bar). (b) The gate voltage effectively results in the tilting of the open surfaces. (c) The tilted surface Brillouin zones lead to the tilting of the Fermi arcs. (d) Two adjacent surfaces with opposite rotation of Fermi arcs induce negative refraction.

Imposing an electric potential on the gates results in penetration of the electric field into the Weyl nanowire, which leads to redistribution of the electrons around the surface.[1] The field penetration depth increases with the gate voltage.[1] Therefore, by imposing a slanted electric potential $V_g(z)$ along the nanowire, the redistribution of the electrons in the nanowire adjusts the bearings of the open surfaces [see Fig. 1(b)]. Due to the screening effect, such a gate voltage has little effect on the bulk states and thus the Weyl nodes. For nanowires with a properly chosen surface bearing relative to the orientation of the bulk Weyl nodes, the electric potential results in an effective tilting of the Fermi arc in each surface Brillouin zone [see Fig. 1(c)]. Such a relative tilting of Fermi arcs in the surface Brillouin zone can lead to perfect negative refraction between adjacent surfaces[33,34] [see Fig. 1(d)]. The surface negative refraction considerably suppresses the conduction of electrons along the nanowire, i.e., for linear Fermi arcs, this effect produces a sharp electrically tunable on/off switch of the conductance. We analyze the adverse impact of dispersive Fermi arcs and the influence of surface disorder. Our proposal offers (i) a robust surface effect that does not necessitate passivation, (ii) reduced dissipation due to the backscattering-free channels, and (iii) a tunable sharp on/off switch. Note that our proposal is still far from being competitive with current FET technologies due to challenges in device fabrication, the required high quality of the Weyl semimetal, and sensitivity to finite temperatures. Nevertheless, it can be used to explore the exotic properties of Weyl semimetals and Fermi arc states and stimulates the research on topological matter toward applications.

In order to realize a WEYLFET with high on/off ratio, it is essential to have ideal Weyl semimetals[35,36] in which the Fermi energy crosses both Weyl points and the transport is dominated by surface electrons. Furthermore, we consider sufficiently small tilting angles such that reduction of the cross section area of the nanowire is negligible. Hence, the main effect of the slanted gate voltage is the tilting of the orientation of the Fermi arcs, and the WEYLFET is controlled by the modulated surface transport.

Instead of studying nanowires with various surface bearings, we focus on the bulk Weyl nanowire with a general orientation of Weyl points, while retaining the same termination configuration of the nanowire. This approach is beneficial for the numerical study of the surface states.[33] More concretely, we consider the minimal inversion ($\mathscr{P}$)-symmetric Weyl semimetal with two generally orientated Weyl points. We start with a Weyl semimetal with two Weyl points at $\pm(0, 0, k_0)$,

$$H(\boldsymbol{k}) = \hbar v(k_x\sigma_x + k_y\sigma_y) + M(k_0^2 - \boldsymbol{k}^2)\sigma_z, \tag{1}$$

where v, M, and k_0 are the parameters, $\boldsymbol{k} = (k_x, k_y, k_z)$ is the wave vector, and $\sigma_{x,y,z}$ are the Pauli matrices acting on the pseudospin space. The general orientation of Weyl points is achieved using the rotational transformation U to the effective Hamiltonian[37] $\mathscr{H}(\boldsymbol{k}) = H\big(U^{-1}\boldsymbol{k}\big)$, e.g., the rotation by an angle φ around the axis $k_x = k_y$, $k_z = 0$ yields two Weyl points located at $\pm k_0(-\frac{\sin\varphi}{\sqrt{2}}, \frac{\sin\varphi}{\sqrt{2}}, \cos\varphi)$. We consider a nanowire along the z-direction with a square cross section with side length L [cf. Fig. 1(b)]. We take $\varphi_0 = \pi/2$ as the starting point in the absence of applied gate voltage $V_g(z)$. The gating results in the rotation of the Weyl points with angle $\varphi_0 - \varphi(V_g)$. It corresponds to a tilting of the Fermi arcs by an angle $\theta(V_g) = \varphi_0 - \tan^{-1}[\tan\varphi(V_g)/\sqrt{2}]$ in the surface Brillouin zone[33] [Fig. 1(d)].

For convenience, we unfold the four open surfaces into the x–z plane and label the longitudinal (transverse) momentum by k_z (k'_x) [see Fig. 1(d)]. The Fermi arcs on surfaces I and II can be described

© Author(s) 2020

by the effective Hamiltonian,

$$H_{\mathrm{I,II}}(\mathbf{k}) = \hbar v_0(\sin\theta k_x' \pm \cos\theta k_z) + \varepsilon_{\mathrm{I,II}}(\mathbf{k}), \tag{2}$$

where $\mathbf{k} = (k_x', k_z)$ is the in-plane momentum, v_0 is the velocity of the surface states, and "±" corresponds to surfaces I and II, respectively. $\varepsilon_{\mathrm{I,II}}$ is the dispersion term, which introduces a finite curvature to the Fermi arcs as in real materials. When $\varepsilon_{\mathrm{I,II}} = 0$, the straight Fermi arcs defined by $H_{\mathrm{I,II}} = \sin\theta k_x' \pm \cos\theta k_z \equiv 0$ have end points at $\pm k_0\left[-(\sin\varphi)/\sqrt{2}, \cos\varphi\right]$ for surface I and at $\pm k_0\left[(\sin\varphi)/\sqrt{2}, \cos\varphi\right]$ for surface II.[33] The two Fermi arcs have opposite tiltings [see Figs. 1(c) and 1(d)]. For a finite tilting angle ($\theta < \pi/2$), the velocity in the z-direction is inverted as the electrons transfer through the boundary between surfaces I and II, leading to negative refraction [see Fig. 1(d)]. This results in full suppression of electrons' flow along the z-direction. This is the key mechanism behind the WEYLFET, i.e., even infinitesimal gating should lead to an on/off control of the electronic transport.

More realistically, Weyl semimetals exhibit dispersive Fermi arcs that depend on both bulk and surface details. Here, we consider a parabolic dispersion $|\varepsilon_{\mathrm{I,II}}| = d[k_0^2(1 - \frac{1}{2}\sin^2\varphi) - k_x'^2 - k_z^2]$, where the overall sign of the dispersive correction on each surface can change. By tuning the dispersion strength $|d|$, the Fermi arcs become curved [cf. Figs. 2(a) and 2(b)], as observed in real materials. Correspondingly, the electronic group velocities $\boldsymbol{v}^{\mathrm{I,II}}(\mathbf{k}) = (v_x^{\mathrm{I,II}}, v_z^{\mathrm{I,II}})$ for the two surface states become $\mathbf{k}$-dependent. The zero-energy single-spin conductance along the wire can be evaluated quasiclassically by

$$G = 2Le^2\rho_0\bar{v}_z, \quad \bar{v}_z = \int_{-k_x^0}^{k_x^0} \frac{dk_x'}{2k_x^0} v_z(k_x') \tag{3}$$

with

$$v_z(k_x') = \frac{v_z^{\mathrm{I}}(k_x', k_z)v_x^{\mathrm{II}}(k_{x2}', k_z) + v_z^{\mathrm{II}}(k_{x2}', k_z)v_x^{\mathrm{I}}(k_x', k_z)}{v_x^{\mathrm{I}}(k_x', k_z) + v_x^{\mathrm{II}}(k_{x2}', k_z)}, \tag{4}$$

where the integral is taken over the incident states of surface I and the velocity $\boldsymbol{v}^{\mathrm{II}}(k_{x2}', k_z)$ is determined by the conservation of k_z during the negative refraction. In Eqs. (3) and (4), ρ_0 is the surface density of states per unit area, $\bar{v}_z$ is the average velocity in the z-direction, and $\pm k_x^0$ are the k_x component of the Weyl points.

For the case of straight Fermi arcs ($d = 0$) with $\theta = 0$, the conductance reduces to $G_0 = 2Le^2\rho_0 v_0$. As the Fermi arcs are tilted by a finite angle $\theta \neq 0$, we have $v_x^{\mathrm{I}} = v_x^{\mathrm{II}}$ and $v_z^{\mathrm{I}} = -v_z^{\mathrm{II}}$, which results in perfect negative refraction [cf. Fig. 1(d)]. As a result, the conductance is completely switched off by the gradient gate voltage, thus realizing a WEYLFET. This result also holds true when finite dispersion is added in the form of $\varepsilon_{\mathrm{I}} = -\varepsilon_{\mathrm{II}}$. In this case, due to the existence of reflection, the negative refraction is imperfect for small θ and results in a finite switch-off angle θ_0 [see Fig. 2(a)].[38]

We also investigate the case with equal dispersion, i.e., $\varepsilon_{\mathrm{I}} = \varepsilon_{\mathrm{II}}$. In this case, the conductance G becomes a function of the tilting angle θ [see Fig. 2(b)].[39] G decreases with θ, indicating the suppression of transport by negative refraction. Whereas for straight Fermi arcs, G exhibits a sharp switch-off, as the dispersion strength increases, the current carried by refracted electrons cannot cancel out the incident current, resulting in a net current, which reduces the on/off ratio of the transistor for small θ.

Complementary to the 2D surface negative refraction analysis above, the on/off switch of the WEYLFET conductance can be understood by studying the 1D band structure of the nanowire. We map the Hamiltonian $\mathscr{H}(\boldsymbol{k})$ onto a cubic lattice through the substitutions $k_i \to a^{-1}\sin k_i a$, $k_i^2 \to 2a^{-2}(1 - \cos k_i a)$, with a being the lattice constant. We can then solve the model and plot its energy bands using KWANT.[40,41] In Fig. 3, we compare the resulting band structures with and without the tilt of the Fermi arcs. For $\theta = 0$, the energy bands contributed by the surface states are gapless, indicating a metallic phase. For finite tilting angle θ, a gap opening occurs for the surface states, and the conduction is switched off for small

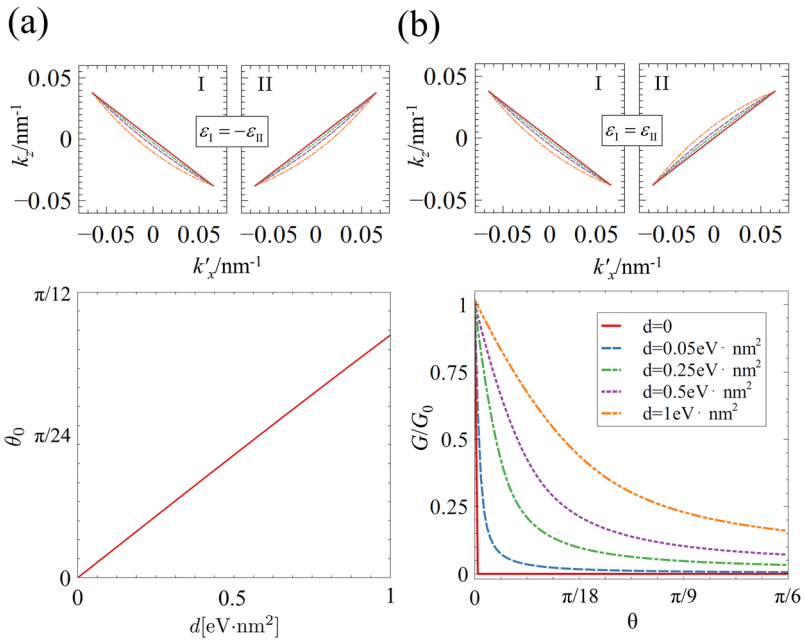

FIG. 2. (a) The Fermi arcs defined by Eq. (2) with different dispersion strengths d [labeled by the legend in (b)] (upper panel) and the switch-off angle θ_0 as a function of d (lower panel) with $\varepsilon_{\mathrm{I}} = -\varepsilon_{\mathrm{II}}$. (b) The Fermi arcs defined by Eq. (2) (upper panel) and the conductance G [Eq. (3)] as a function of θ (lower panel) with different dispersion d and $\varepsilon_{\mathrm{I}} = \varepsilon_{\mathrm{II}}$. All results are obtained with parameters: $v_0 = 10^6$ m/s and $k_0 = 0.1$ nm^{-1}.

© Author(s) 2020

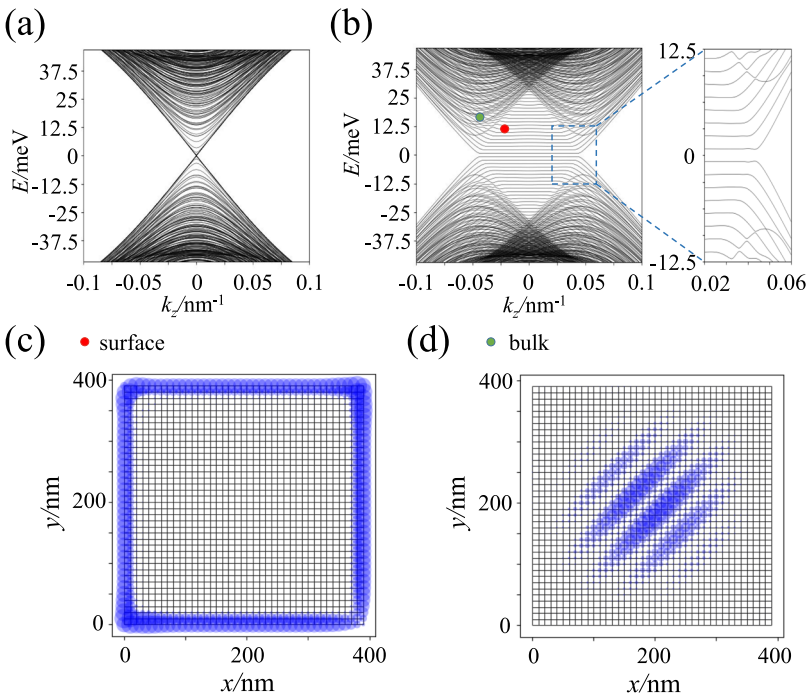

FIG. 3. Band structure of the Weyl nanowire for (a) $\theta = 0$ and (b) $\theta = \pi/6$, numerically calculated with a cross section of 40 × 40 sites. Spatial distribution of (c) a surface state and (d) a bulk state. Parameters used are $a = 10$ nm, $k_0 = 0.1$ nm^{-1}, $M = 4.375$ eV nm^2, and $v = 10^6$ m/s.

bias voltages. Therefore, under a small bias voltage, the WEYLFET corresponds to a gate-tunable gap closing and opening in the 1D picture, which is consistent with the 2D picture of negative refraction [cf. Fig. 1(d)]. Note that the gap here is small (≈1 meV), which limits the utilization of the WEYLFET at finite temperatures. At a finite temperature, the current can be carried by thermally excited electrons above the gap, which reduces the on/off ratio of the switch. This conclusion is consistent with the quasiclassical picture of the surface transport because at finite energy, the Fermi arcs on two adjacent surfaces shift toward the opposite direction and only part of the electrons can undergo negative refraction. A larger gap can be achieved by increasing the tilting angle θ or by reducing the cross section of the nanowire.

Next, we numerically calculate the conductance through the nanowire based on the cubic lattice model.[40,41] We introduce surface dispersion using an on-site potential U on the surface layer; because the surface states have a **k**-dependent spatial distribution perpendicular to the surface, the on-site potential leads to a **k**-dependent potential or equivalently to an effective dispersion of the Fermi arcs. The conductance along the nanowire as a function of the tilting angle θ of the Fermi arcs is shown in Figs. 4(a) and 4(b). In Fig. 4(a), the onsite potential U takes opposite values on adjacent surfaces. Therefore, the dispersion on adjacent surfaces also takes opposite values, i.e., $\varepsilon_{\mathrm{I}} = -\varepsilon_{\mathrm{II}}$, and the on/off effect is confirmed. The angle at which the conductance is completely switched off increases with the onsite potential U because curved Fermi arcs imply that reflection processes exist in addition to negative refraction for small θ. Hence, in order to realize perfect negative refraction, the tilting angle must exceed a critical value [cf. Fig. 2(a)]. In Fig. 4(b), the onsite potential U takes the same value on all surfaces and the dispersions on the surfaces also become the same, i.e., $\varepsilon_{\mathrm{I}} = \varepsilon_{\mathrm{II}}$. As a result, the on/off ratio is reduced as U increases, which is in good agreement with the results in Fig. 2(b). Note that, here too, the surface dispersion has an adverse effect on the WEYLFET performance, which reduces the on/off ratio of the device. Therefore, in order to make a WEYLFET with high efficiency, it is preferable to use Weyl semimetals with weak and opposite surface dispersions. Recent experiments have realized Fermi arc manipulation by surface decoration,[42,43] which paves the way to realize our proposal.

In real materials, surface roughness is unavoidable, and we simulate this effect by including surface disorder. For $\mathscr{P}$-symmetric Weyl semimetals, the corresponding chiral surface states imply that electronic transport is immune to surface disorder, i.e., the functionality of the WEYLFET should be robust to disorder. In Figs. 4(c) and 4(d), we present the calculated device conductance under different surface disorder strengths V for both dispersion configurations ($U_{\mathrm{I}} = \pm U_{\mathrm{II}}$). The length of the disordered region in the z-direction is $40a$. In both cases, the conductance decreases as surface disorder becomes stronger. This stems from the enhancement of backscattering that is induced by the disorder. However, the surface disorder has no effect on the switch-off region in Fig. 4(c), where perfect negative refraction occurs. In other words, the surface disorder has little effect on the functionality of the WEYLFET and the on/off ratio remains almost the same.

So far, we have solely analyzed a minimal $\mathscr{P}$-symmetric Weyl semimetal containing two Weyl points. Onto this minimal model, we have introduced the general principle of gate tunable Fermi arc tilting that can lead to negative refraction. Nevertheless, further work will analyze even more realistic situations, including (i) Weyl semimetals with multiple pairs of Weyl points, as in most of the materials;[21–32] here, the geometry of the nanowire should be properly chosen such that the overlap between the projections of different

© Author(s) 2020

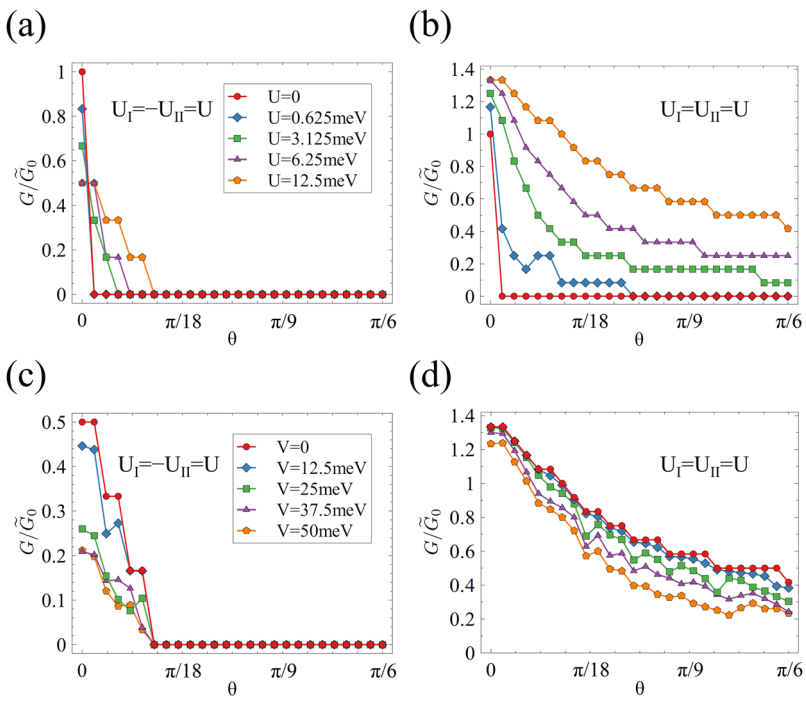

FIG. 4. Numerical simulation of the adverse effect on the WEYLFET performance. (a) and (b) The conductance G for different surface dispersions renormalized by $\widetilde{G}_0$ with $U = 0$ and $\theta = 0$. (c) and (d) The conductance G in the presence of surface disorder with $U = 12.5$ meV. All other parameters are the same as those in Fig. 3.

Fermi arcs to the z-axis is minimized. Otherwise, the reflection at the boundary between different surfaces reduces the potency of negative refraction and accordingly the on/off ratio of the WEYLFET. (ii) For time-reversal symmetric Weyl semimetals, the Fermi arc states are not chiral, leading to enhanced backscattering. In this case, we expect that surface disorder will have a stronger impact and will reduce the on/off ratio of the WEYLFET. Hence, for the time-reversal symmetric Weyl semimetal, a nanowire with a clean surface is required for a high-efficiency WEYLFET. (iii) Another adverse effect can arise from the deviation of the Fermi level from the bulk Weyl points. In this case, bulk electrons participate in the transport and contribute an overall background to the conductance, which reduces the on/off ratio of the WEYLFET. At the same time, multiple scattering may occur in the bulk states, which also increases the dissipation of the WEYLFET. Furthermore, the finite bulk density of states also brings a considerable screening effect, which reduces the efficiency of the slanted gate voltage. Based on these observations, ideal Weyl semimetals are needed for efficient WEYLFETs,[35,36] similar to their vital role in measuring other properties of Weyl semimetals. (iv) Finally, in many Weyl semimetals, the Fermi arcs' dispersion is complex, making these surface states not much different from 2D normal metals, which cannot be used for WEYLFETs. Consequently, the material candidate for the WEYLFET should contain short Fermi arcs with a small curvature.[44–46]

In summary, we have explored a possible application of Weyl semimetal as a field-effect transistor (WEYLFET), which is based on the electronic negative refraction between Fermi arcs on the surface of the device. By using the gradient gate along the Weyl nanowire, an on/off switch of the conductance can be achieved with a high ratio. Ideal Weyl semimetals with vanishing bulk density of states, chiral surface channels, and a small Fermi arc curvature can serve as good candidates for such a high-efficiency WEYLFET with low-power consumption.

We acknowledge financial support from the Swiss National Science Foundation (SNSF) through Division II and the Careers Division.

REFERENCES

[1] C. Galup-Montoro *et al.*, *MOSFET Modeling for Circuit Analysis and Design* (World Scientific, 2007).
[2] A. Javey, J. Guo, Q. Wang, M. Lundstrom, and H. Dai, "Ballistic carbon nanotube field-effect transistors," Nature **424**, 654 (2003).
[3] F. Schwierz, "Graphene transistors," Nat. Nanotechnol. **5**, 487 (2010).
[4] F. D. M. Haldane, "Model for a quantum Hall effect without Landau levels: Condensed-matter realization of the "parity anomaly"," Phys. Rev. Lett. **61**, 2015–2018 (1988).
[5] C.-X. Liu, X.-L. Qi, X. Dai, Z. Fang, and S.-C. Zhang, "Quantum anomalous Hall effect in $Hg_{1-y}Mn_yTe$ quantum wells," Phys. Rev. Lett. **101**, 146802 (2008).
[6] R. Yu, W. Zhang, H.-J. Zhang, S.-C. Zhang, X. Dai, and Z. Fang, "Quantized anomalous Hall effect in magnetic topological insulators," Science **329**, 61–64 (2010).
[7] M. Z. Hasan and C. L. Kane, "Colloquium: Topological insulators," Rev. Mod. Phys. **82**, 3045 (2010).
[8] X.-L. Qi and S.-C. Zhang, "Topological insulators and superconductors," Rev. Mod. Phys. **83**, 1057 (2011).
[9] C.-Z. Chang, J. Zhang, X. Feng, J. Shen, Z. Zhang, M. Guo, K. Li, Y. Ou, P. Wei, L.-L. Wang, Z.-Q. Ji, Y. Feng, S. Ji, X. Chen, J. Jia, X. Dai, Z. Fang, S.-C. Zhang, K. He, Y. Wang, L. Lu, X.-C. Ma, and Q.-K. Xue, "Experimental observation of the quantum anomalous Hall effect in a magnetic topological insulator," Science **340**, 167–170 (2013).
[10] C.-X. Liu, S.-C. Zhang, and X.-L. Qi, "The quantum anomalous Hall effect: Theory and experiment," Annu. Rev. Condens. Matter Phys. **7**, 301–321 (2016).

© Author(s) 2020

[11] X.-R. Chen, W. Chen, L. B. Shao, and D. Y. Xing, "Engineering chiral edge states in two-dimensional topological insulator/ferromagnetic insulator heterostructures," Phys. Rev. B **99**, 085417 (2019).
[12] X. Wan, A. M. Turner, A. Vishwanath, and S. Y. Savrasov, "Topological semimetal and Fermi-arc surface states in the electronic structure of pyrochlore iridates," Phys. Rev. B **83**, 205101 (2011).
[13] S. Murakami, "Phase transition between the quantum spin Hall and insulator phases in 3D: Emergence of a topological gapless phase," New J. Phys. **9**, 356 (2007).
[14] A. A. Burkov and L. Balents, "Weyl semimetal in a topological insulator multilayer," Phys. Rev. Lett. **107**, 127205 (2011).
[15] Z. Wang, H. Weng, Q. Wu, X. Dai, and F. Zhong, "Three-dimensional Dirac semimetal and quantum transport in Cd_3As_2," Phys. Rev. B **88**, 125427 (2013).
[16] H. Weng, C. Fang, F. Zhong, B. Andrei Bernevig, and X. Dai, "Weyl semimetal phase in noncentrosymmetric transition-metal monophosphides," Phys. Rev. X **5**, 011029 (2015).
[17] S.-M. Huang, S.-Y. Xu, I. Belopolski, C.-C. Lee, G. Chang, B. K. Wang, N. Alidoust, G. Bian, M. Neupane, C. Zhang *et al.*, "A Weyl fermion semimetal with surface fermi arcs in the transition metal monopnictide TaAs class," Nat. Commun. **6**, 7373 (2015).
[18] K.-Yu Yang, Y.-M. Lu, and Y. Ran, "Quantum Hall effects in a Weyl semimetal: Possible application in pyrochlore iridates," Phys. Rev. B **84**, 075129 (2011).
[19] C.-K. Chan, N. H. Lindner, R. Gil, and P. A. Lee, "Photocurrents in Weyl semimetals," Phys. Rev. B **95**, 041104 (2017).
[20] G. B. Osterhoudt, L. K. Diebel, M. J. Gray, Xu Yang, J. Stanco, X. Huang, B. Shen, Ni Ni, P. J. W. Moll, Y. Ran *et al.*, "Colossal mid-infrared bulk photovoltaic effect in a type-I Weyl semimetal," Nat. Mater. **18**, 471 (2019).
[21] B. Q. Lv, H. M. Weng, B. B. Fu, X. P. Wang, H. Miao, J. Ma, P. Richard, X. C. Huang, L. X. Zhao, G. F. Chen *et al.*, "Experimental discovery of Weyl semimetal TaAs," Phys. Rev. X **5**, 031013 (2015).
[22] S.-Y. Xu, I. Belopolski, N. Alidoust, M. Neupane, G. Bian, C. Zhang, R. Sankar, G. Chang, Z. Yuan, C.-C. Lee *et al.*, "Discovery of a Weyl fermion semimetal and topological fermi arcs," Science **349**, 613–617 (2015).
[23] S.-Y. Xu, N. Alidoust, I. Belopolski, Z. Yuan, G. Bian, T.-R. Chang, H. Zheng, V. N. Strocov, D. S. Sanchez, G. Chang *et al.*, "Discovery of a Weyl fermion state with fermi arcs in niobium arsenide," Nat. Phys. **11**, 748 (2015).
[24] S.-Y. Xu, I. Belopolski, D. S. Sanchez, C. Zhang, G. Chang, C. Guo, G. Bian, Z. Yuan, H. Lu, T.-R. Chang *et al.*, "Experimental discovery of a topological Weyl semimetal state in tap," Sci. Adv. **1**, e1501092 (2015).
[25] N. Xu, H. M. Weng, B. Q. Lv, C. E. Matt, J. Park, F. Bisti, V. N. Strocov, D. Gawryluk, E. Pomjakushina, K. Conder *et al.*, "Observation of Weyl nodes and fermi arcs in tantalum phosphide," Nat. Commun. **7**, 11006 (2016).
[26] K. Deng, G. Wan, P. Deng, K. Zhang, S. Ding, E. Wang, M. Yan, H. Huang, H. Zhang, Z. Xu *et al.*, "Experimental observation of topological fermi arcs in type-II Weyl semimetal $MoTe_2$," Nat. Phys. **12**, 1105 (2016).
[27] L. X. Yang, Z. K. Liu, Y. Sun, H. Peng, H. F. Yang, T. Zhang, B. Zhou, Y. Zhang, Y. F. Guo, M. Rahn *et al.*, "Weyl semimetal phase in the non-centrosymmetric compound TaAs," Nat. Phys. **11**, 728 (2015).
[28] L. Huang, T. M. McCormick, M. Ochi, Z. Zhao, M.-T. Suzuki, R. Arita, Y. Wu, D. Mou, H. Cao, J. Yan *et al.*, "Spectroscopic evidence for a type II Weyl semimetallic state in $MoTe_2$," Nat. Mater. **15**, 1155 (2016).
[29] A. Tamai, Q. S. Wu, I. Cucchi, F. Y. Bruno, S. Riccò, T. K. Kim, M. Hoesch, C. Barreteau, E. Giannini, C. Besnard *et al.*, "Fermi arcs and their topological character in the candidate type-II Weyl semimetal $MoTe_2$," Phys. Rev. X **6**, 031021 (2016).
[30] J. Jiang, Z. K. Liu, Y. Sun, H. F. Yang, C. R. Rajamathi, Y. P. Qi, L. X. Yang, C. Chen, H. Peng, C. C. Hwang *et al.*, "Signature of type-II Weyl semimetal phase in $MoTe_2$," Nat. Commun. **8**, 13973 (2017).
[31] I. Belopolski, D. S. Sanchez, Y. Ishida, X. Pan, P. Yu, S.-Y. Xu, G. Chang, T.-R. Chang, H. Zheng, N. Alidoust *et al.*, "Discovery of a new type of topological Weyl fermion semimetal state in $Mo_xW_{1-x}Te_2$," Nat. Commun. **7**, 13643 (2016).
[32] B. Q. Lv, N. Xu, H. M. Weng, J. Z. Ma, P. Richard, X. C. Huang, L. X. Zhao, G. F. Chen, C. E. Matt, F. Bisti *et al.*, "Observation of Weyl nodes in TaAs," Nat. Phys. **11**, 724 (2015).
[33] G. Chen, O. Zilberberg, and W. Chen, "Negative refraction between fermi arc surface states in Weyl semimetals," e-print arXiv:1911.04941 [cond-mat.mes-hall] (2019).
[34] H. He, C. Qiu, L. Ye, X. Cai, X. Fan, M. Ke, F. Zhang, and Z. Liu, "Topological negative refraction of surface acoustic waves in a Weyl phononic crystal," Nature **560**, 61 (2018).
[35] J. Ruan, S.-K. Jian, H. Yao, H. Zhang, S.-C. Zhang, and D. Xing, "Symmetry-protected ideal Weyl semimetal in HgTe-class materials," Nat. Commun. **7**, 11136 (2016).
[36] J. Ruan, S.-K. Jian, D. Zhang, H. Yao, H. Zhang, S.-C. Zhang, and D. Xing, "Ideal Weyl semimetals in the chalcopyrites $CuTlSe_2$, $AgTlTe_2$, $AuTlTe_2$, and $ZnPbAs_2$," Phys. Rev. Lett. **116**, 226801 (2016).
[37] W. Chen, L. Jiang, R. Shen, L. Sheng, B. G. Wang, and D. Y. Xing, "Specular Andreev reflection in inversion-symmetric Weyl semimetals," Europhys. Lett. **103**, 27006 (2013).
[38] The switch-off angle θ_0 is given by $\theta_0 = \arctan \frac{v_0}{\sqrt{2}k_0 d}$ for the effective Hamiltonian [Eq. (2)].
[39] For curved Fermi arcs and small θ, there exist reflection processes in addition to the negative refraction. Here, the reflection does not change v_z and we calculate $\bar{v}_z$ by $\bar{v}_z = \int_{-k_x^0}^{k_x^1} \frac{dk_x}{2k_x^0} \frac{v_x^{\mathrm{I}} v_z^{\mathrm{II}} + v_z^{\mathrm{II}} v_x^{\mathrm{I}}}{v_x^{\mathrm{I}} + v_x^{\mathrm{II}}} + \int_{k_x^1}^{k_x^0} \frac{dk_x}{2k_x^0} v_z^{\mathrm{I}}$, where $k_x^1 = -k_0 \sin\theta/\sqrt{1+\sin^2\theta} + \hbar v_0 \cos\theta/d$ separates the Fermi arc into two segments which lead to negative refraction and reflection, respectively.
[40] C. W. Groth, M. Wimmer, A. R. Akhmerov, and X. Waintal, "Kwant: A software package for quantum transport," New J. Phys. **16**, 063065 (2014).
[41] See github.com/GUANGZECHEN/WEYLFET/ for open access to the python scripts for the numerical simulations.
[42] H. F. Yang, L. X. Yang, Z. K. Liu, Y. Sun, C. Chen, H. Peng, M. Schmidt, D. Prabhakaran, B. A. Bernevig, C. Felser *et al.*, "Topological Lifshitz transitions and fermi arc manipulation in Weyl semimetal NbAs," Nat. Commun. **10**, 3478 (2019).
[43] N. Morali, R. Batabyal, P. Kumar Nag, E. Liu, Q. Xu, Y. Sun, B. Yan, C. Felser, N. Avraham, and H. Beidenkopf, "Fermi-arc diversity on surface terminations of the magnetic Weyl semimetal $Co_3Sn_2S_2$," Science **365**(6459), 1286–1291 (2019) .
[44] J. Li, L. Yang, S. Du, Z. Wang, B.-L. Gu, S.-C. Zhang, K. He, W. Duan, and Y. Xu, "Intrinsic magnetic topological insulators in van der Waals layered $MnBi_2Te_4$-family materials," Sci. Adv. **5**, eaaw5685 (2019).
[45] L.-L. Wang, N. H. Jo, B. Kuthanazhi, Y. Wu, R. J. McQueeney, K. Adam, and P. C. Canfield, "Single pair of Weyl fermions in the half-metallic semimetal $EuCd_2As_2$," Phys. Rev. B **99**, 245147 (2019).
[46] J.-R. Soh, F. de Juan, M. G. Vergniory, N. B. M. Schröter, M. C. Rahn, D. Y. Yan, M. Bristow, P. A. Reiss, J. N. Blandy, Y. F. Guo *et al.*, "An ideal Weyl semimetal induced by magnetic exchange," Phys. Rev. B **100**, 201102 (2019).

© Author(s) 2020